J Biomol NMR (2016) 64:1–7
DOI 10.1007/s10858-015-0004-y

COMMUNICATION

Accurate measurement of $^{3}J_{HNH\alpha}$ couplings in small or disordered proteins from WATERGATE-optimized TROSY spectra

Julien Roche[1] · Jinfa Ying[1] · Ad Bax[1]

Received: 17 October 2015 / Accepted: 30 November 2015 / Published online: 10 December 2015

Abstract Provided that care is taken in adjusting the WATERGATE element of a ^{1}H–^{15}N TROSY-HSQC experiment, such that neither the water magnetization nor the $^{1}H^{\alpha}$ protons are inverted by its final 180° pulse, $^{3}J_{HNH\alpha}$ couplings can be measured directly from splittings in the ^{1}H dimension of the spectrum. With band-selective ^{1}H decoupling, very high ^{15}N resolution can be achieved. A complete set of $^{3}J_{HNH\alpha}$ values, ranging from 3.4 to 10.1 Hz was measured for the 56-residue third domain of IgG-binding protein G (GB3). Using the H–N–C^{α}–H^{α} dihedral angles extracted from a RDC-refined structure of GB3, $^{3}J_{HNH\alpha}$ values predicted by a previously parameterized Karplus equation agree to within a root-mean-square deviation (rmsd) of 0.37 Hz with the experimental data. Values measured for the Alzheimer's implicated $A\beta^{1-40}$ peptide fit to within an rmsd of 0.45 Hz to random coil $^{3}J_{HNH\alpha}$ values.

Keywords Abeta · IDP · Karplus curve · Random coil · Synuclein · Protein NMR

$^{3}J_{HNH\alpha}$ values have long been recognized as important parameters for defining the backbone torsion angles, ϕ, in peptides and proteins (Bystrov 1976; Pardi et al. 1984). Parameterization of best-fitting Karplus curves typically has been carried out using $^{3}J_{HNH\alpha}$ couplings measured for small proteins and dihedral angles taken from the corresponding high resolution X-ray structures, yielding root-mean-square deviations (rmsd's) in the 0.8–1.0 Hz range (Pardi et al. 1984; Ludvigsen et al. 1991; Vuister and Bax 1993). Considering that in such X-ray structures, the electron density of the hydrogens is often ill defined, these atoms are typically model-built into the structure, assuming idealized geometry. Alternatively, the H–N–C^{α}–H^{α} dihedral angles needed as input to the Karplus equation are directly calculated from $\phi_i - 60°$, where ϕ_i is the backbone torsion angle of residue i, defined by the backbone atoms C'_{i-1}, N_i, C^{α}_i, and C'_i. The residual rmsd in the fit was initially believed to result from difficulties in measuring $^{3}J_{HNH\alpha}$ at an accuracy better than about 0.8 Hz, but a large number of conceptually rather different methods, ranging from addition and subtraction of in-phase and anti-phase $^{1}H^{N}$–{$^{1}H^{\alpha}$} doublets (Ludvigsen et al. 1991), E.COSY measurements (Griesinger et al. 1987; Wang and Bax 1996; Montelione and Wagner 1989), quantitative J correlation methods (Vuister and Bax 1993; Lohr et al. 1999), fitting of J_{HH}-modulated 2D HSQC and HMQC spectra (Billeter et al. 1992; Kuboniwa et al. 1994), to multiple quantum methods (Rexroth et al. 1995), were unable to go significantly below this 0.8 Hz threshold. Only when using the actual H–N–C^{α}–H^{α} dihedral angles, with ^{1}H positions determined by measurement of residual dipolar couplings (RDCs), as input to the Karplus equation, were rmsd's well below 0.5 Hz obtained (Vogeli et al. 2007; Maltsev et al. 2014). This result indicates that the earlier, higher rmsd values were dominated by deviations from idealized geometries, in particular the assumption of the amide hydrogen being located in the peptide plane.

Julien Roche and Jinfa Ying have contributed equally to this work.

Electronic supplementary material The online version of this article (doi:10.1007/s10858-015-0004-y) contains supplementary material, which is available to authorized users.

✉ Ad Bax
bax@nih.gov

[1] Laboratory of Chemical Physics, National Institute of Diabetes and Digestive and Kidney Diseases, National Institutes of Health, Bethesda, MD 20892, USA

Here we demonstrate that for small or intrinsically disordered proteins $^{3}J_{HNH\alpha}$ can be measured conveniently and at high accuracy from a 2D ^{1}H–^{15}N TROSY-HSQC spectrum (Pervushin et al. 1997, 1998; Schulte-Herbruggen and Sorensen 2000). However, as discussed below, care must be taken in adjustment of the pulses that normally have a "water flip-back" function, such that they also invert the $^{1}H^{\alpha}$ resonances. Appropriate choice of the flip back pulses will suppress $^{3}J_{HNH\alpha}$-modulation during the last phase of the magnetization transfer from ^{15}N to ^{1}H, preventing an antiphase contribution to the $^{1}H^{N}$–$\{^{1}H^{\alpha}\}$ doublet line shape. When ^{1}H–^{15}N TROSY-HSQC spectra are recorded on protonated proteins, unresolvable $^{2}J_{H\alpha N}$, $^{3}J_{H\alpha N}$, and $^{3}J_{H\beta N}$ splittings can limit the attainable resolution in small or intrinsically disordered protein, and it then is useful to remove such splittings by insertion of a band-selective decoupling pulse at the mid-point of the ^{15}N evolution period.

The pulse scheme of the water-flip-back ^{1}H–^{15}N TROSY-HSQC experiment is shown in Fig. 1 and it is essentially the same as the original ^{1}H–^{15}N TROSY-HSQC experiment (Pervushin et al. 1998; Schulte-Herbruggen and Sorensen 2000), except for the decoupling pulse applied to the aliphatic protons at time point c. Note that this decoupling pulse is implemented as a combination of an H^{N}-selective 180° pulse, using an IBURP2 shape (Geen and Freeman 1991), followed by a non-selective offset-compensated composite 180° pulse (Levitt and Freeman 1981). Together, this pulse pair inverts all ^{1}H except for $^{1}H^{N}$, yielding a convenient and effective method for decoupling aliphatic protons during ^{15}N evolution (Bruschweiler et al. 1988). In order to permit ^{15}N coherence encoding without introducing the requirement of a large frequency-dependent phase correction in the ^{15}N dimension, a short gradient encoding period (using gradients G_3 and G_4, separated by a ^{15}N 180° pulse at time point b) is inserted in the standard manner (Kay et al. 1992). To avoid the need for a frequency-dependent phase correction in the ^{1}H dimension, the last pair of $^{1}H/^{15}N$ 180° pulses are slightly offset relative to one another: By applying the last non-selective ^{1}H 180° pulse (time point g) a short time, $\varepsilon \approx 150$ µs, after the ^{15}N 180° pulse (time point f), full $^{1}H^{N}$ chemical shift refocusing after the last simultaneous pair of $^{1}H/^{15}N$ 90° pulses (time point e) is delayed by 2ε, whereas $^{1}J_{NH}$ rephasing is active for the regular duration, $2\delta = {}^{1}/(2{}^{1}J_{NH}) \approx 5.3$ ms. This permits insertion of the last pulsed field gradient decoding pulse after the last ^{15}N 90° pulse, before $^{1}H^{N}$ chemical shifts are refocused at time point h, which completes the ST2-PT polarization transfer (Pervushin et al. 1998). Water suppression is very effective with this pulse scheme, also on cryogenic probeheads, due to the combined effects of water-flip-back (Grzesiek and Bax 1993), the WATERGATE element (Piotto et al. 1992b), and coherence selection (Kay et al. 1992).

$^{3}J_{HNH\alpha}$ dephasing during the initial INEPT magnetization transfer from $^{1}H^{N}$ to ^{15}N (prior to time point a) and during the first half of the final ST2-PT element, between time points d and e, only results in very slight attenuation

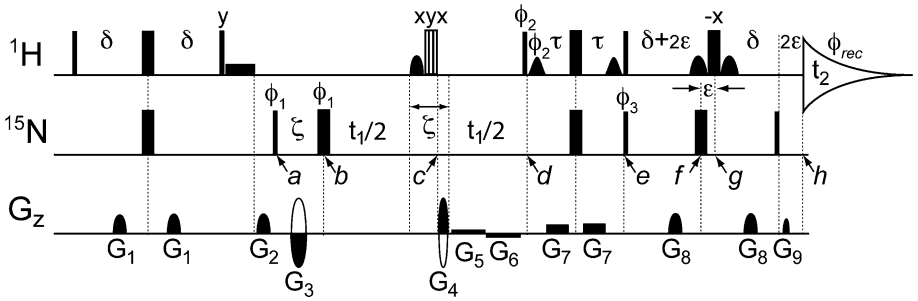

Fig. 1 Pulse scheme of the water-flip-back ^{1}H–^{15}N TROSY-HSQC experiment. The *narrow* and *wide filled bars* represent the hard 90° and 180° pulses, while the vertically hatched *open bar* is a $90_x210_y90_x$ composite 180° ^{1}H pulse. The *filled rectangular box* before the G_2 gradient pulse is a 1-ms rectangular water-flipback pulse that returns the solvent magnetization to +z after the INEPT transfer. The shaped pulse applied for the band selective decoupling in the middle of t_1 has an IBURP2 (Geen and Freeman) shape (1.1 ms duration at 800 MHz), is applied to H^{N} and centered 3.6 ppm downfield from the H_2O resonance. Two water-flipback pulses (center lobe of a sinc profile, 1.0 ms) are applied between time points d and e to ensure the water magnetization returns to +z at time point e. At time point g, two sine-bell shaped pulses (600 µs) flanking the non-selective 180° ^{1}H pulse are used to keep the water magnetization at +z, and to refocus $^{3}J_{HNH\alpha}$ evolution during the 2δ+4ε delay. All pulses are applied along x unless otherwise indicated. Durations of all shaped pulses are for a ^{1}H frequency of 800 MHz and should be scaled inversely relative to this frequency if applied at higher or lower magnetic fields. Delay durations: $\delta = 2.65$ ms; $\varepsilon = 150$ µs; $\zeta = 2081$ µs; $\tau \approx 2.1$ ms [shorter than $1/(4{}^{1}J_{NH})$ to minimize the ^{15}N anti-TROSY component (Schulte-Herbruggen and Sorensen 2000)]. Phase cycling: $\phi_1 = y, x, -y, -x$; $\phi_2 = y$; $\phi_3 = y$; $\phi_{rec} = y, -x, -y, x$. To obtain the second FID for the echo-antiecho quadrature detection, the following phase cycling is used together with inversion of the G_3 and G_4 gradient pulses: $\phi_1 = y, -x, -y, x$; $\phi_2 = -y$; $\phi_3 = -y$. These phase parameters pertain to Bruker spectrometers; for Varian/Agilent spectrometers y and −y should be interchanged. Gradients are sine-bell or *rectangular shaped*, as marked in the figure, with durations: $G_{1,2,3,4,5,6,7,8,9} = 0.977$, 1.2, 1.1, 0.9, $t_1/4$, $t_1/4$, 1.086, 0.977, 0.202 ms, and strengths of 21.7, 28.7, −41.3, 41.3, 0.91, −0.91, 2.1, 25.9, 41.3 G/cm

of the final signal intensity at time point h (by a factor of ca. $\cos[2\pi\ {}^3J_{HNH\alpha}\ \delta]\{1 + \cos[2\pi\ {}^3J_{HNH\alpha}\ \tau]\}/2$) and creation of multiple quantum $^1H^N$–$^1H^\alpha$ coherences that will remain invisible during detection. This dephasing prior to time point e therefore may be safely ignored. However, $^3J_{HNH\alpha}$ dephasing between time points e and h will remain intact if only the non-selective ^1H 180° pulse were applied at time point g. Refocusing of the $^3J_{HNH\alpha}$ dephasing at time point h is achieved if only the $^1H^N$ is inverted by the 180° pulse at time point g. In practice, this can be accomplished by again using the combination of a non-selective 180° pulse, followed or preceded by a selective $^1H^\alpha$ inversion pulse, which forms the basis for band-selective homonuclear (BASH) decoupling (Bruschweiler et al. 1988; Ying et al. 2014). In Pervushin's ST2-PT implementation of the TROSY experiment, this last non-selective ^1H 180° pulse is already surrounded by two water-selective 90° flip-back pulses, ensuring that the water magnetization is minimally impacted by this combination of ^1H pulses, essentially constituting a WATERGATE element when surrounded by the standard pair of pulsed field gradients (Piotto et al. 1992a). $^1H^\alpha$ spins that resonate close to the H_2O resonance therefore are also minimally affected by the soft/hard pulse combination, centered at time point g.

The width of the $^1H^\alpha$ region not affected by the soft/hard pulse combination is remarkably wide, due to the offset-compensating effect of this symmetric $90°_x$, $180°_{-x}$, $90°_x$ composite pulse (Levitt and Freeman 1979; Shaka and Freeman 1983). For example, Fig. 2 compares the inversion profile for the case where the non-selective $180°_{-x}$ pulse is applied just prior to two back-to-back sine-bell-shaped 600-μs $90°_x$ pulses with the profile obtained when the $180°_{-x}$ is applied in between these two pulses, as in the TROSY scheme of Fig. 1. As can be seen, the non-inversion profile of the $90°_x$, $180°_{-x}$, $90°_x$ pulse combination has a favorable shape, leaving z magnetization above 85 % (i.e., inverting less than ~7.5 % of the H^α spins) for offsets up to ±640 Hz, and >90 % inversion of z magnetization (i.e., inverting >95 % of the ^1H spins) at offsets ≥2100 Hz. These bandwidths are inversely proportional to the duration of the shaped $90°_x$ pulses. Pulse shapes different from a sine bell, e.g. Gaussian shapes, can be used to fine tune the inversion profile. Even a single sine-bell shaped soft $180°_{-x}$ pulse, with a non-selective ^1H 180° pulse superimposed at its mid-point gives a desirable inversion profile (red line in Fig. 2). In practice, we use the two sine-bell shaped $90°_x$ pulses separated by the non-selective 180°

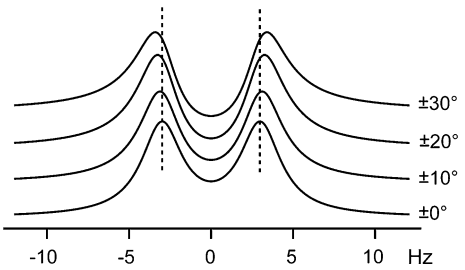

Fig. 3 Illustration of the effect of $^3J_{HH}$ phase modulation prior to the start of ^1H data acquisition on the apparent splitting. Simulated data are shown for a doublet with $^3J_{HH} = 6$ Hz, marked by the *dashed lines*. The *bottom* doublet corresponds to the absence of phase modulation, with vertically displaced doublets having phase errors of ±10, ±20, and ±30°. The apparent splitting, as measured from the maxima of the two components, increases approximately linearly with the phase error. Note that the phase error introduced by the ca 5.5-ms $^3J_{HH}$ modulation during the final half of the ST2-PT transfer for a 6 Hz $^3J_{HH}$ coupling is only ±6°, but is responsible for the differences in apparent $^3J_{HH}$ shown in Fig. 5b

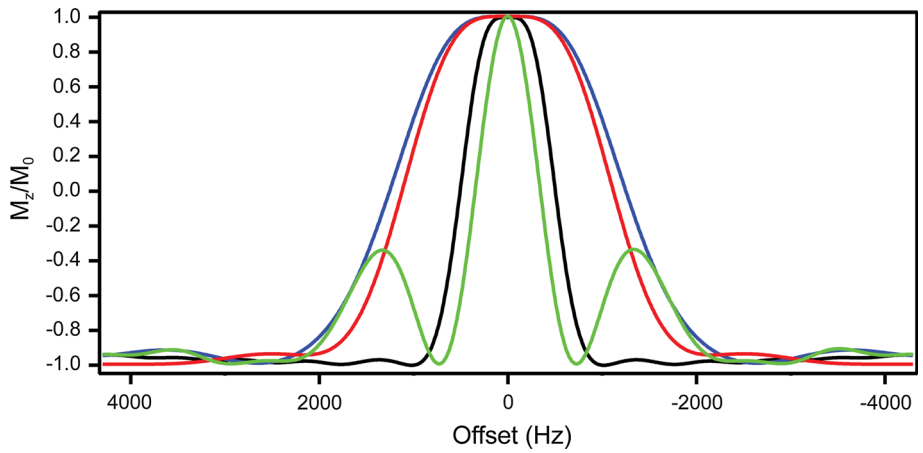

Fig. 2 Inversion profile, M_z/M_o, as a function of resonance offset for different hard-soft pulse combinations, all using a 20 μs hard 180° pulse. *Black line* $90°_x$, $180°_{-x}$, $90°_x$, where the $90°_x$ pulses are sine-bell shaped with a duration of 1.5 ms each. *Blue* $90°_x$, $180°_{-x}$, $90°_x$, where the $90°_x$ pulses are sine-bell shaped with a duration of 0.6 ms each. *Red* $90°_x$, $180°_{-x}$, $90°_x$, where the first and second $90°_x$ pulse have the shape of the left half and of the right half of a sine-bell, respectively, and a duration of 0.6 ms each. For comparison, the *green line* corresponds to the inversion profile of a $90°_x$, $90°_x$, $180°_{-x}$ combination, with 0.6-ms sine-bell shaped $90°_x$ pulses

pulse as a compromise between an optimal inversion profile and a minimal total duration of this pulse combination. In principle, a REBURP 180° $^{1}H^{N}$ pulse (Geen and Freeman 1991) could be used instead of the 90°$_{x}$, 180°$_{-x}$, 90°$_{x}$ pulse combination, but in practice we find the use of such a pulse less effective at optimizing suppression of the H_2O signal.

In the absence of selective $^{1}H^{\alpha}$ inversion, the phase of the two $^{1}H^{N}$–{$^{1}H^{\alpha}$} doublet components at time point h in Fig. 1 is given by $\pm 2\pi\ ^{3}J_{HNH\alpha}(\delta + 2\varepsilon)$. Although relatively small (ca $\pm k°$ for a $^{3}J_{HNH\alpha}$ coupling of k Hz and $2\delta + 4\varepsilon = 5.9$ ms), such an antiphase dispersive contribution, which is not easily visible to the eye, will increase the apparent splitting, as measured from the maximum height position of each doublet component, by ca $k \times LW/90$, where LW is the average line width of each doublet component (Fig. 3). So, the error introduced in the measured $^{3}J_{HNH\alpha}$ coupling when J-modulation is not suppressed is approximately proportional to both the size of the $^{3}J_{HNH\alpha}$ coupling and to the $^{1}H^{N}$ line width. For a typical $^{3}J_{HNH\alpha}$ coupling of 7.5 Hz and a digitally enhanced line width of 3 Hz, this therefore would result in an overestimate of the measured coupling by ca 0.25 Hz. However, as described above, this contribution is easily suppressed by adjusting the duration of the shaped 90°$_{x}$ ^{1}H pulses such that the $^{1}H^{\alpha}$ spins are not inverted. Note that the small error

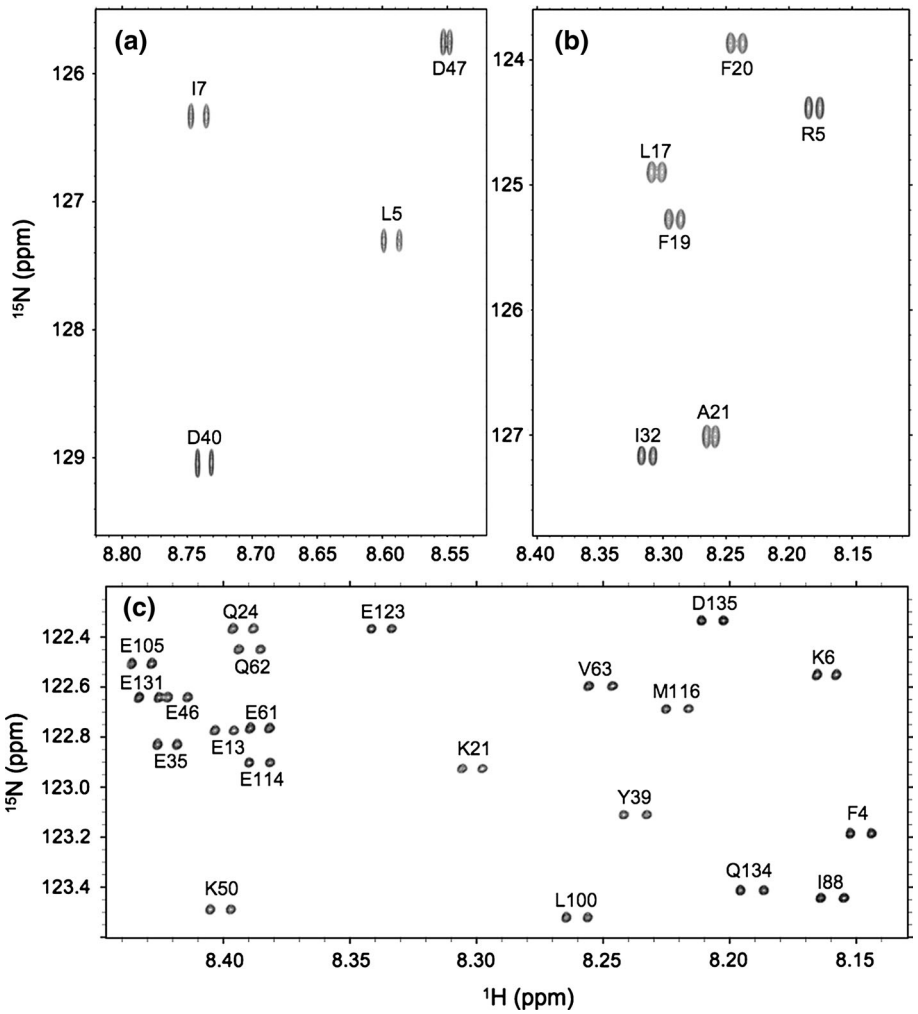

Fig. 4 Expanded small regions of the 800 MHz ^{1}H–^{15}N TROSY-HSQC spectra recorded for samples of **a** 1.2 mM GB3 in 100 mM NaCl, 25 mM sodium phosphate, pH 6.4, 293 K; **b** 150 μM $A\beta^{1-40}$ in 20 mM sodium phosphate, pH 7.0, 277 K; and **c** 300 μM α-synuclein in 25 mM sodium phosphate, pH 6.0, 288 K. Spectra were recorded with acquisition times of 284 ms (t_2) and 128 ms (t_1) for $A\beta^{1-40}$; 393 ms (t_2) and 74 ms (t_1) for GB3; and 393 ms (t_2) and 1016 ms (t_1) for α-synuclein, all using 0.6-ms sine-bell shaped pulses surrounding the last non-selective 180° pulse. For $A\beta^{1-40}$ and α-synuclein the carrier frequency was moved upfield by 0.3 ppm relative to the H_2O resonance position only during application of the last ^{1}H 90°$_{x}$, 180°$_{-x}$, 90°$_{x}$ pulse combination, and for the remainder of the pulse sequences the ^{1}H carrier was positioned on the H_2O resonance. Spectra were resolution-enhanced in the ^{1}H dimension using a Lorentzian-to-Gaussian enhancement function, and processed and peak-picked with the NMRPipe software package (Delaglio et al. 1995)

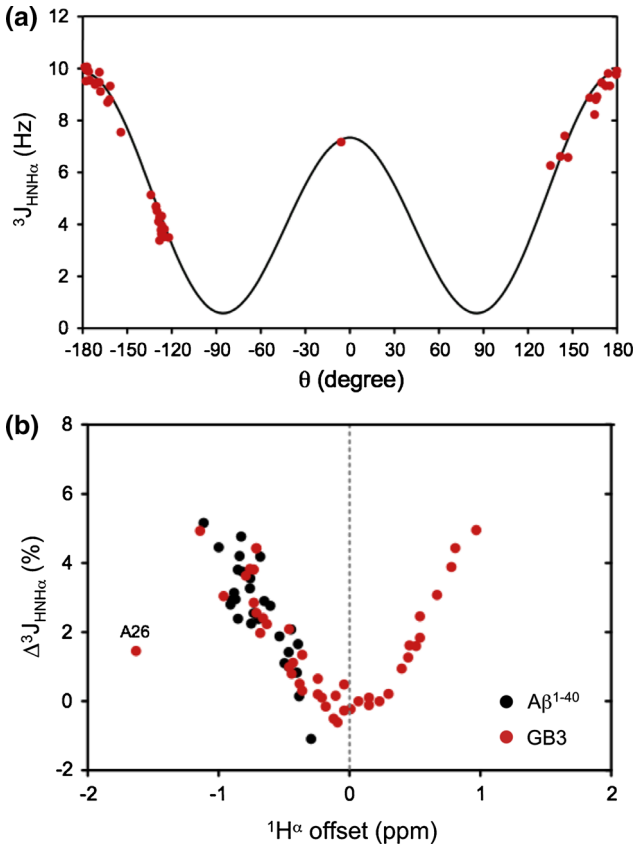

Fig. 5 Measurement of $^3J_{HNH\alpha}$ couplings from the HSQC-TROSY spectra of Fig. 4. **a** Plot of the GB3 $^3J_{HNH\alpha}$ values (Table S1) as a function of the H–N–C^α–H^α dihedral angle, θ, derived from a RDC-refined structure (PDB entry 2N7J), using the Karplus equation parameterization $^3J_{HNH\alpha} = 7.97 \times \cos^2\theta - 1.26 \times \cos\theta + 0.63$ (Vogeli et al. 2007). Mobile residues L12 and D40 were not included in the fit. **b** Fractional difference $\Delta^3J_{HNH\alpha} = [^3J_{HNH\alpha}(1.5\text{ ms}) - {}^3J_{HNH\alpha}(0.6\text{ ms})]/^3J_{HNH\alpha}(0.6\text{ ms})$, where $^3J_{HNH\alpha}(1.5\text{ ms})$ and $^3J_{HNH\alpha}(0.6\text{ ms})$ are the values measured using 1.5-ms and 0.6-ms duration 90° water-flip back pulses around the last ^1H 180° pulse. $\Delta^3J_{HNH\alpha}$ values are plotted as a function of the $^1H^\alpha$ chemical shift offset relative to the frequency at which the radiofrequency carrier is positioned during the final $90°_x$, $180°_{-x}$, $90°_x$ pulse combination. $\Delta^3J_{HNH\alpha}$ values measured for $A\beta^{1-40}$ are in black, GB3 values in *red*. Note that for the far upfield shifted GB3 A26 resonance, neither measurement suppresses $^3J_{HNH\alpha}$ modulation, and both yield a slight over-estimate of the true coupling, and therefore a small $\Delta^3J_{HNH\alpha}$

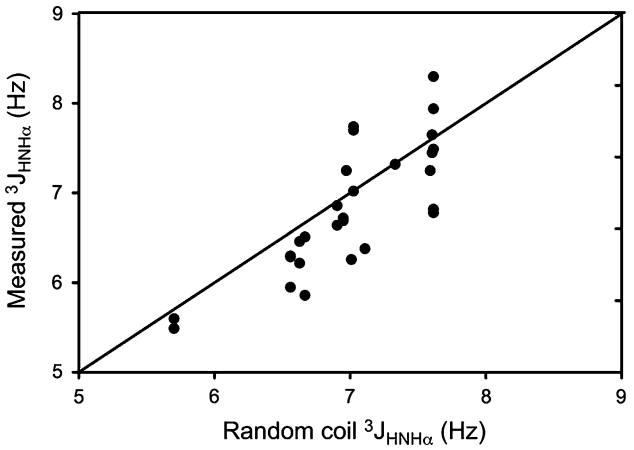

Fig. 6 Plot of $^3J_{HNH\alpha}$ values measured for $A\beta^{1-40}$ against "random coil" values, derived from the residue-specific averages observed for IDP α-synuclein (Maltsev et al. 2012). The $A\beta^{1-40}$ $^3J_{HNH\alpha}$ couplings are reported in SI Table S2. The rmsd between observed and random coil $^3J_{HNH\alpha}$ couplings equals 0.45 Hz, and the Pearson's correlation coefficient, R_P is 0.8

introduced by *J* modulation is distinct from the apparent decrease caused by the finite lifetime of the $^1H^\alpha$ spin states, i.e., by the dependence on their selective inversion recovery rates (Harbison 1993). This latter effect can become quite significant in larger proteins, where zero frequency spectral density and therefore ^1H–^1H spin flip rates are high. It then needs to be accounted for either computationally (Vuister and Bax 1993; Ball et al. 2013), or by altering the pulse scheme (Rexroth et al. 1995). For the smaller systems to which the TROSY-HSQC $^3J_{HNH\alpha}$ measurement is applicable, such as GB3, the effect tends to be minor, resulting in a small systematic difference of only ~0.12 Hz relative to the values measured previously (Vogeli et al. 2007) with a multi-quantum pulse scheme that was designed to suppress the effect.

Figure 4 shows three small regions of the ^1H–^{15}N TROSY-HSQC spectra of GB3, the $A\beta^{1-40}$ peptide, and α-synuclein. For the latter two, the $^1H^\alpha$ spins all resonate upfield of the ^1H_2O water resonance and the ^1H carrier is shifted upfield by 0.3 ppm during application of the final $90°_x$, $180°_{-x}$, $90°_x$ pulse combination, such as to shift the band where $^1H^\alpha$ spins are not inverted upfield relative to the H_2O resonance. For GB3 at 293 K, where H_2O resonates approximately at the center of the H^α region, no such frequency shift was used. As can be seen from the spectra, well resolved doublets are readily obtained for these proteins, whose $^1H^N$ line widths are significantly reduced by the TROSY effect (ca 1.5 to twofold at 800 MHz ^1H frequency) over regular HSQC spectra, i.e. by relaxation interference between the $^1H^N$ chemical shift anisotropy (CSA) and the ^{15}N–^1H dipolar relaxation mechanisms.

With an rmsd of only 0.37 Hz, $^3J_{HNH\alpha}$ couplings measured for GB3 from the TROSY-HSQC spectrum (Supplementary Table S1) agree very well with the previously parameterized Karplus equation (Vogeli et al. 2007) when using a recent RDC-refined structure of this protein (PDB entry 2N7J) to derive the dihedral angles, confirming the accuracy of our $^3J_{HNH\alpha}$ measurements (Fig. 5a).

As mentioned above, the error in the apparent $^3J_{HNH\alpha}$ splitting that exists when J modulation is not suppressed is proportional to the size of $^3J_{HNH\alpha}$. Figure 5b shows the fractional difference (as a percentage of the actually measured $^3J_{HNH\alpha}$ coupling) between values measured from two

^{1}H–^{15}N TROSY-HSQC spectra: one using 1.5 ms 90° shaped sine bell pulses and one using 0.6-ms pulses. The first measurement corresponds to 50 % inversion of the $^{1}H^{\alpha}$ spins at resonance offsets of $\sim\pm505$ Hz relative to the carrier, and nearly complete suppression of J modulation over a $\sim\pm260$ Hz bandwidth. For the measurement with 0.6-ms pulses, these bandwidths are 2.5 times larger. As can be seen in Fig. 5b, when the J modulation is fully suppressed in both measurements, i.e., at small offsets, the fractional difference between the two sets is essentially zero. However, at ±810 Hz the fractional difference reaches a maximum, before again decreasing for large offsets (e.g. residue A26 at 3.19 ppm) where neither measurement was effective at suppressing J modulation.

Measurements of $^{3}J_{HNH\alpha}$ couplings are quite useful in the analysis of residual structure in IDPs, where they represent a particularly unambiguous reporter on the time- or ensemble-average of the ϕ angles.

We note that ^{1}H–^{15}N TROSY-HSQC spectra that are free of $^{3}J_{HNH\alpha}$ phase modulation errors can also be generated with the powerful BEST-TROSY pulse scheme, which then additionally yields sensitivity enhancement over the scheme of Fig. 1 (Favier and Brutscher 2011; Solyom et al. 2013). However, addition of aliphatic ^{1}H decoupling during ^{15}N evolution (Fig. 1) is somewhat incompatible with the spirit of the BEST type experiments, which aim to avoid inversion of the aliphatic protons. Achieving the highest possible ^{15}N resolution is often paramount, as illustrated for the most crowded region of the α-synuclein spectrum (Fig. 4c), and we therefore opted to modify the standard TROSY-HSQC pulse sequence instead. Note that, as applies for most experiments for $^{3}J_{HNH\alpha}$ measurement, hydrogen exchange with water causes line broadening in the $^{1}H^{N}$ dimension (and for TROSY type experiments such as the present one also in the ^{15}N dimension) by an amount k_{ex}/π Hz, which can become a factor limiting the smallest couplings that can be measured.

A number of computational studies (Sgourakis et al. 2011; Ball et al. 2011, 2013, 2014; Rosenman et al. 2013) strongly rely on a set of relatively incomplete $^{3}J_{HNH\alpha}$ values measured for $A\beta^{1-40}$ and $A\beta^{1-42}$ by various groups (Hou et al. 2004; Yan et al. 2008; Sgourakis et al. 2007; Waelti et al. 2015). Here, we have demonstrated that these couplings can be measured at very high precision and good accuracy in such systems, at a very high level of completeness. The only missing values are for the N-terminal residue and two His residues, which exhibit rapid exchange and concomitant broadening of their resonances, and the Gly residues, for which the $^{3}J_{HNH\alpha2}$ and $^{3}J_{HNH\alpha3}$ couplings give rise to triplet splitting patterns from which only the sum of their two $^{3}J_{HNH\alpha}$ couplings can be measured. Although, with a Pearson's correlation coefficient of $R_P = 0.8$, the values reported here for $A\beta^{1-40}$ (Supplementary Table S2) correlate well with random coil $^{3}J_{HNH\alpha}$ values (Maltsev et al. 2012) derived for IDP α-synuclein (Fig. 6), significant deviations are also seen. For example, values for V12 (6.78 Hz) and V24 (6.82 Hz) fall well below the 7.6-Hz random coil value of this β-branched residue, whereas V18 (8.30 Hz) and V39 (7.94 Hz) show significantly elevated values. Analysis of these couplings, in concert with other types of J couplings, chemical shifts, and NOEs, is currently on-going in our group in an effort to obtain quantitative, residue-specific ϕ/ψ distributions using the recently introduced MERA program (Mantsyzov et al. 2015).

Acknowledgments We thank Dennis A. Torchia for useful discussions, and Jung Ho Lee for preparing the sample used for Fig. 4c. This work was supported by the Intramural Research Program of the National Institute of Diabetes and Digestive and Kidney Diseases and the Intramural Antiviral Target Program of the Office of the Director, NIH.

References

Ball KA, Phillips AH, Nerenberg PS, Fawzi NL, Wemmer DE, Head-Gordon T (2011) Homogeneous and heterogeneous tertiary structure ensembles of amyloid-beta peptides. Biochemistry 50:7612–7628

Ball KA, Phillips AH, Wemmer DE, Head-Gordon T (2013) Differences in beta-strand populations of monomeric A beta 40 and A beta 42. Biophys J 104:2714–2724

Ball KA, Wemmer DE, Head-Gordon T (2014) Comparison of structure determination methods for intrinsically disordered amyloid-beta peptides. J Phys Chem B 118:6405–6416

Billeter M, Neri D, Otting G, Qian YQ, Wuthrich K (1992) Precise vicinal coupling-constants 3J(HN-HA) in proteins from nonlinear fits of J-modulated [15N, 1H]-COSY experiments. J Biomol NMR 2:257–274

Bruschweiler R, Griesinger C, Sørensen OW, Ernst RR (1988) Combined use of hard and soft pulses for omega-1 decoupling in two-dimensional NMR spectroscopy. J Magn Reson 78:178–185

Bystrov VF (1976) Spin–spin couplings and the conformational states of peptide systems. Prog NMR Spectrosc 10:41–81

Delaglio F, Grzesiek S, Vuister GW, Zhu G, Pfeifer J, Bax A (1995) NMRpipe—a multidimensional spectral processing system based on Unix pipes. J Biomol NMR 6:277–293

Favier A, Brutscher B (2011) Recovering lost magnetization: polarization enhancement in biomolecular NMR. J Biomol NMR 49:9–15

Geen H, Freeman R (1991) Band-selective radiofrequency pulses. J Magn Reson 93:93–141

Griesinger C, Sørensen OW, Ernst RR (1987) Practical aspects of the E.COSY technique. Measurement of scalar spin-spin coupling constants in peptides. J Magn Reson 75:474–492

Grzesiek S, Bax A (1993) The importance of not saturating H_2O in protein NMR. Application to sensitivity enhancement and NOE measurement. J Am Chem Soc 115:12593–12594

Harbison GS (1993) Interference between J-couplings and cross-relaxation in solution NMR-spectroscopy—consequences for macromolecular structure determination. J Am Chem Soc 115:3026–3027

Hou LM, Shao HY, Zhang YB, Li H, Menon NK, Neuhaus EB, Brewer JM, Byeon IJL, Ray DG, Vitek MP, Iwashita T, Makula

RA, Przybyla AB, Zagorski MG (2004) Solution NMR studies of the A beta(1–40) and A beta(1–42) peptides establish that the met35 oxidation state affects the mechanism of amyloid formation. J Am Chem Soc 126:1992–2005

Kay LE, Keifer P, Saarinen T (1992) Pure absorption gradient enhanced heteronuclear single quantum correlation spectroscopy with improved sensitivity. J Am Chem Soc 114:10663–10665

Kuboniwa H, Grzesiek S, Delaglio F, Bax A (1994) Measurement of H^N–H^α J couplings in calcium-free calmodulin using new 2D and 3D water-flip-back methods. J Biomol NMR 4:871–878

Levitt MH, Freeman R (1979) NMR population-inversion using a composite pulse. J Magn Reson 33:473–476

Levitt MH, Freeman R (1981) Compensation for pulse imperfections in NMR spin-echo experiments. J Magn Reson 43:65–80

Lohr F, Schmidt JM, Ruterjans H (1999) Simultaneous measurement of (3)J(HN, H alpha) and (3)J(H alpha, H beta) coupling constants in C-13, N-15-labeled proteins. J Am Chem Soc 121:11821–11826

Ludvigsen S, Andersen KV, Poulsen FM (1991) Accurate measurements of coupling-constants from 2-dimensional nuclear-magnetic-resonance spectra of proteins and determination of phi-angles. J Mol Biol 217:731–736

Maltsev AS, Ying JF, Bax A (2012) Impact of N-terminal acetylation of α-synuclein on its random coil and lipid binding properties. Biochemistry 51:5004–5013

Maltsev AS, Grishaev A, Roche J, Zasloff M, Bax A (2014) Improved cross validation of a static ubiquitin structure derived from high precision residual dipolar couplings measured in a drug-based liquid crystalline phase. J Am Chem Soc 136:3752–3755

Mantsyzov AB, Shen Y, Lee JH, Hummer G, Bax A (2015) MERA: a webserver for evaluating backbone torsion angle distributions in dynamic and disordered proteins from NMR data. J Biomol NMR 63:85–95

Montelione GT, Wagner G (1989) Accurate measurements of homonuclear H–N–H–alpha coupling-constants in polypeptides using heteronuclear 2D NMR experiments. J Am Chem Soc 111:5474–5475

Pardi A, Billeter M, Wüthrich K (1984) Calibration of the angular dependence of the amide proton-C^α proton coupling constants, $^3J_{HN\alpha}$, in a globular protein: use of $^3J_{HN\alpha}$ for identification of helical secondary structure. J Mol Biol 180:741–751

Pervushin K, Riek R, Wider G, Wuthrich K (1997) Attenuated T-2 relaxation by mutual cancellation of dipole- dipole coupling and chemical shift anisotropy indicates an avenue to NMR structures of very large biological macromolecules in solution. Proc Natl Acad Sci USA 94:12366–12371

Pervushin KV, Wider G, Wuthrich K (1998) Single transition-to-single transition polarization transfer (ST2-PT) in [N15, H1]-TROSY. J Biomol NMR 12:345–348

Piotto M, Saudek V, Sklenar V (1992a) Gradient-tailored excitation for single-quantum NMR-spectroscopy of aqueous-solutions. J Biomol NMR 2:661–665

Piotto M, Saudek V, Sklenár V (1992b) Gradient-tailored excitation for single-quantum NMR spectroscopy of aqueous sloutions. J Biomol NMR 2:661–665

Rexroth A, Schmidt P, Szalma S, Geppert T, Schwalbe H, Griesinger C (1995) New principle for the determination of coupling-constants that largely suppresses differential relaxation effects. J Am Chem Soc 117:10389–10390

Rosenman DJ, Connors CR, Chen W, Wang C, Garcia AE (2013) A beta monomers transiently sample oligomer and fibril-like configurations: ensemble characterization using a combined MD/NMR approach. J Mol Biol 425:3338–3359

Schulte-Herbruggen T, Sorensen OW (2000) Clean TROSY: compensation for relaxation-induced artifacts. J Magn Reson 144:123–128

Sgourakis NG, Yan Y, McCallum SA, Wang C, Garcia AE (2007) The Alzheimer's peptides A beta 40 and 42 adopt distinct conformations in water: a combined MD/NMR study. J Mol Biol 368:1448–1457

Sgourakis NG, Merced-Serrano M, Boutsidis C, Drineas P, Du Z, Wang C, Garcia AE (2011) Atomic-level characterization of the ensemble of the A beta(1–42) monomer in water using unbiased molecular dynamics simulations and spectral algorithms. J Mol Biol 405:570–583

Shaka AJ, Freeman R (1983) Composite pulses with dual compensation. J Magn Reson 55:487–493

Solyom Z, Schwarten M, Geist L, Konrat R, Willbold D, Brutscher B (2013) BEST-TROSY experiments for time-efficient sequential resonance assignment of large disordered proteins. J Biomol NMR 55:311–321

Vogeli B, Ying JF, Grishaev A, Bax A (2007) Limits on variations in protein backbone dynamics from precise measurements of scalar couplings. J Am Chem Soc 129:9377–9385

Vuister GW, Bax A (1993) Quantitative *J* correlation: a new approach for measuring homonuclear three-bond $J(H^NH^\alpha)$ coupling constants in ^{15}N-enriched proteins. J Am Chem Soc 115:7772–7777

Waelti MA, Orts J, Voegeli B, Campioni S, Riek R (2015) Solution NMR studies of recombinant A beta(1–42): from the presence of a micellar entity to residual beta-sheet structure in the soluble species. ChemBioChem 16:659–669

Wang AC, Bax A (1996) Determination of the backbone dihedral angles phi in human ubiquitin from reparametrized empirical Karplus equations. J Am Chem Soc 118:2483–2494

Yan Y, McCallum SA, Wang C (2008) M35 oxidation induces A beta 40-like structural and dynamical changes in A beta 42. J Am Chem Soc 130:5394–5395

Ying J, Roche J, Bax A (2014) Homonuclear decoupling for enhancing resolution and sensitivity in NOE and RDC measurements of peptides and proteins. J Magn Reson 241:97–102